Hindawi Publishing Corporation
Journal of Nanomaterials
Volume 2010, Article ID 562035, 12 pages
doi:10.1155/2010/562035

Review Article

Optical Properties and Immunoassay Applications of Noble Metal Nanoparticles

Shaoli Zhu and Wei Zhou

School of Mechanical & Aerospace Engineering, Precision Engineering & Nanotechnology Centre, Nanyang Technological University, Singapore 639798

Correspondence should be addressed to Shaoli Zhu, slzhu@ntu.edu.sg

Received 13 October 2009; Revised 17 February 2010; Accepted 2 April 2010

Academic Editor: Zhi-Li Xiao

Noble metal, especially gold (Au) and silver (Ag) nanoparticles exhibit unique and tunable optical properties on account of their surface plasmon resonance (SPR). In this paper, we mainly discussed the theory background of the enhanced optical properties of noble metal nanoparticles. Mie theory, transfer matrix method, discrete dipole approximation (DDA) method, and finite-difference time domain (FDTD) method applied brute-force computational methods for different nanoparticles optical properties. Some important nanostructure fabrication technologies such as nanosphere lithography (NSL) and focused ion beam (FIB) are also introduced in this paper. Moreover, these fabricated nanostructures are used in the plasmonic sensing fields. The binding signal between the antibody and antigen, amyloid-derived diffusible ligands (ADDLs)-potential Alzheimer's disease (AD) biomarkers, and staphylococcal enterotixn B (SEB) in nano-Moore per liter (nM) concentration level are detected by our designed nanobiosensor. They have many potential applications in the biosensor, environment protection, food security, and medicine safety for health, and so forth, fields.

1. Introduction

The intense scattering and absorption of light from noble metal nanoparticles is the source of the beautiful colors in stained glass windows and has attracted the interest of scientists for generations. Although scientists have learned that the characteristic hues of these noble metal nanoparticle suspensions arise from their strong interaction with light, the advent of the field of nanoparticle optics has allowed for a deeper understanding of the relationship among material properties (including chemical composition, size, and shape), local dielectric environments, and the observed color of a metal suspension. An understanding of the optical properties of noble metal nanoparticles is of both fundamental and practical significance. It helps to systematically explore the nanoscale structural and local environmental characteristics that cause optical property variation as well as provide access to regimes of predictable behavior. Practically, the tunable optical properties of nanostructures can be applied as materials for surface-enhanced spectroscopy [1], optical filters [2], plasmonic devices [3], and sensors [4].

Noble metal nanoparticles exhibit a strong UV-vis absorption band that is not present in the spectrum of the bulk metals [5]. This absorption band results when the incident photon frequency is resonant with the collective oscillation of the conduction electrons and is known as the localized surface plasmon resonance (LSPR). LSPR excitation results in wavelength selective absorption with extremely large molar extinction coefficients $\sim 3 \times 10^{11}\,\mathrm{M}^{-1}\,\mathrm{cm}^{-1}$ [6], resonant Rayleigh scattering [7, 8] with an efficiency equivalent to that of 10^6 fluorophors [9, 10], and the enhanced local electromagnetic fields near the surface of the nanoparticle which are responsible for the intense signals observed in all surface-enhanced spectroscopies [11].

It is well established that the peak extinction wavelength, $\lambda_{\max}$, of the LSPR spectrum is dependent upon the size, shape, and interparticle spacing of the nanoparticle as well as its dielectric properties and those of the local environments [5]. Consequently, there are at least four

different nanoparticle-based sensing mechanisms that enable the transduction of macromolecular or chemical binding events into optical signals based on changes in the LSPR extinction or scattering intensity, shifts in LSPR $\lambda_{\max}$, or both. These mechanisms are (1) resonant Rayleigh scattering from nanoparticle labels in a manner analogous to fluorescent dye labels [12]; (2) nanoparticle aggregation [13]; (3) charge-transfer interactions at nanoparticle surfaces [14, 15]; and (4) local refractive index changes [16].

In recent years, some research groups are working on developing biosensors based on the localized surface plasmon resonance (LSPR) exhibited by golden metal nanoparticles. The representative works have been performed and reported by the *Van Duyne* Group of Northwestern University [17, 18]. Golden metal nanoparticles with different materials, sizes, periods, and refractive index of the medium around the nanoparticles can scatter the light of different wavelengths according to their characteristic SPR [19]. The target molecules such as proteins or virus can bind to the surface of the metal after chemical prefunction of the nanoparticles [20].

Discrete dipole approximation (DDA) [21, 22] and finite-difference time domain (FDTD) [23, 24] are the widely used designed methods for the nanoparticles used for the LSPR nanobiosensor. Nanosphere lithography (NSL) [25] and focused ion beam (FIB) [26, 27] have been applied widely in the nanofabrication filed. Based on the previous research work, various optical structures have been designed and investigated for plasmon biosensing. This article will mainly review the optical properties and immunoassay applications of noble metal nanoparticles. Emphasis will be given to the description of the theory background of plasmon resonance for metal nanoparticles. In particular, we will focus on the mathematical background and calculated results of DDA and FDTD methods. The fabrication results based on our extend nanofabrication techniques (etc. NSL and FIB) will be revealed too. Examples of detecting various types of biomolecules based on refractive-index plasmonic sensing principle will be presented.

2. Theory Background

As a first approximation, the plasmon resonance for a small spherical metal nanoparticle can be understood by a simple Drude free-electron model, assuming that the positively charged metal atoms are fixed in place and that the valence electrons are dispersed throughout a solid sphere of overall positive charge. In the quasistatic limit, where the wavelength of light is much larger than the size of the particle, the force exerted by the electromagnetic field of the incident light moves all the free-electrons collectively. Using the boundary condition that the electric field is continuous across the surface of the sphere, the static polarizability can be expressed as

$$\alpha = 4\pi R^2 \frac{\varepsilon - \varepsilon_m}{\varepsilon + 2\varepsilon_m}, \tag{1}$$

where R is the sphere radius, ε is the complex dielectric function of the metal and ε_m is the dielectric constant of the embedding medium. The polarizability shows a resonance when the denominator is minimized, which occurs when the magnitude of the real part of the complex dielectric function, ε real, is $-2\varepsilon_m$. This resonance condition for the polarizability leads to a strong extinction of light at the plasmon resonance frequency. Within this free-electron description, plasmons can be thought of as collective oscillations of the conduction-band electrons induced by an interacting light wave.

To determine the plasmon-resonant properties of arbitrarily shaped particles, solutions to Maxwell's equations must be obtained. For nanoparticles with a spherical symmetry, Mie scattering theory [28, 29] provides a rigorous solution that describes well the optical spectra of spheres of any size. To determine the extinction spectrum of a nanoparticle using the theory, the electromagnetic fields of the incident wave, scattered wave and the wave inside the particle are expressed as the sum of a series of vector spherical harmonic basis functions. The electromagnetic fields must then satisfy Maxwell's boundary conditions of continuity at the junction between the nanoparticle and the embedding medium. Mie scattering theory is exact and it accounts for field-retardation effect that becomes significant for particles whose sizes are comparable to the wavelength of light.

For nonspherical geometries, brute-force computational methods, such as the discrete dipole approximation (DDA) [19] and the finite-difference time domain (FDTD) [30, 31] methods are widely used. In the DDA, the scattering and absorption properties of arbitrarily shaped nanostructures are calculated by approximating the complete nanostructure as a finite array of polarizable point dipoles. In response to an external field, the points acquire a dipole moment, and the scattering properties are then calculated as the interaction of a finite number of closely spaced dipoles.

2.1. Mathematical Background and Calculated Results of DDA. DDA algorithm is a powerful numerical method for calculating scattering and absorption for the targets of arbitrary structures. The target is represented as a lattice of polarizable cubic elements (N point dipoles) whose positions and polarizabilities are denoted as r_i and α_i. The electrodynamics of this array of dipoles in the presence of an applied plane wave field is then solved exactly. To do this, the polarization induced in each dipole as a result of the incident and retarded fields from the other elements can be expressed as [21, 22]

$$P_i = \alpha_i E_{\mathrm{loc},i}(r_i), \quad i = 1, 2, \ldots, N, \tag{2}$$

where the local field $E_{\mathrm{loc}}(r_i)$ is the sum of the incident and retarded fields of the other $N - 1$ dipoles. For a given wavelength λ, the field can be expressed as

$$\begin{aligned} E_{\mathrm{loc},i}(r_i) &= E_{\mathrm{inc},i} + E_{\mathrm{retard},i} \\ &= E_0 \exp(ikr_i) - \sum_{\substack{j=1 \\ j \neq i}}^{N} A_{ij} P_j, \quad i = 1, 2, \ldots, N, \end{aligned} \tag{3}$$

where E_0 and $k = 2\pi/\lambda$ are the amplitude and wave number of the incident wave, respectively. The interaction matrix A is then expressed as

$$A_{ij}P_j = \frac{\exp\left(ikr_{ij}\right)}{{r_{ij}}^3} \times \left\{k^2 r_{ij} \times \left(r_{ij} \times P_j\right) + \frac{1 - ikr_{ij}}{{r_{ij}}^2} \times \left[{r_{ij}}^2 P_j - 3r_{ij}\left(r_{ij}P_j\right)\right]\right\}, \quad i = 1, 2, \ldots, N, \; j = 1, 2, \ldots, N, \; j \neq i, \tag{4}$$

where $r_{ij} = |r_i - r_j|$ is the distance vector from dipole i to dipole j. Substituting (3) and (4) into (2), and rearranging the (2), we obtain

$$(\alpha^{-1})P_i + \sum_{\substack{j=1 \\ j \neq i}}^{N} A_{ij}P_j = E_{\text{inc},i}, \quad i = 1, 2, \ldots, N. \tag{5}$$

The polarization vectors and electric fields are then obtained by solving $3N$ linear equations of the form

$$A'P = E, \tag{6}$$

where the off diagonal elements of the matrix, A'_{ij}, is the same as A_{ij}, and the diagonal element of the matrix, A'_{ii}, is α^{-1}. After obtaining the polarization vector $\mathbf{P}$, we can calculate cross section of the extinction as

$$C_{\text{ext}} = \frac{4\pi k}{|E_0|^2} \sum_{i=1}^{N} \text{Im}(E_{\text{loc},i}P_i). \tag{7}$$

The computer time used in the DDA method is proportional to the number of the dipoles. Depending on the error tolerance in the calculation, the typical cube size required for convergence (for a noble metal particle) is in the range of 0.5–2 nm, and the method is limited to the calculation of a particle or a cluster of particles whose total size is a few hundred nanometers in each dimension. For a periodic array of particles, the local electric field and polarization is a periodic function in two dimensions. So we need to solve the linear equations for a single unit cell only. But for the sum term in (3), it is extended to include periodic replicas of as many cells as the numbers, which is needed to converge the expansion.

The extended DDA program of calculating extinction spectra for the two-dimensional infinite arrays is proposed according to the structure character of the rhombic structure while the original DDA program can only calculate extinction spectra of the single particle. The original DDA program DDSCAT 6.1 is from Draine and Flatau, the dielectric constants for gold and silver are taken from [32]. All of our results are calculated by taking the effective index of medium as the external dielectric material and the interdipole spacing is set to be 2 nm in our calculation.

We designed the geometry parameter of the nanostructure array and proposed calculating the extinction spectra of rhombic hybrid Au-Ag nanostructures using DDA aided design method [33]. Using this aided method, a hybrid Au-Ag nanostructures array is designed with the determinant parameters of thickness (Au5 nm, Ag25 nm), period (400 nm) and the refractive index sensitivity (400 nm/RIU). This study shows that the particle material, period and the effective refractive indexes of the mediums have significant effect on the optical properties of the nanostructures, and DDA aided design method can provide the right structure parameters for our hybrid nanostructures. The nanostructure array and the calculated results are shown in Figures 1, 2, 3, 4, and 5. From the above calculations, it is found that the hybrid Au-Ag rhombic nanostructure array can play the role of tuning the plasmon peak with high refractive index sensitivity. In summary, we have proposed a DDA aided design method to determine the thickness, period, and refractive index of the hybrid Au-Ag rhombic nanostructure.

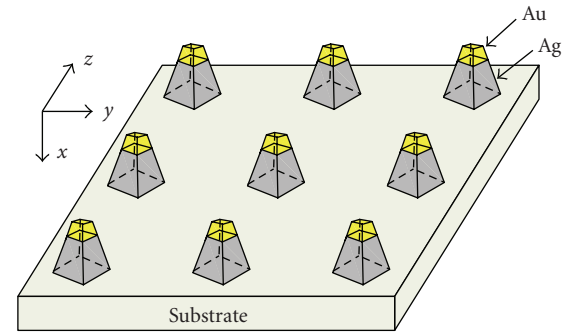

Figure 1: The symmetry two-dimensional infinite rhombic Au-Ag nanostructures. From [33].

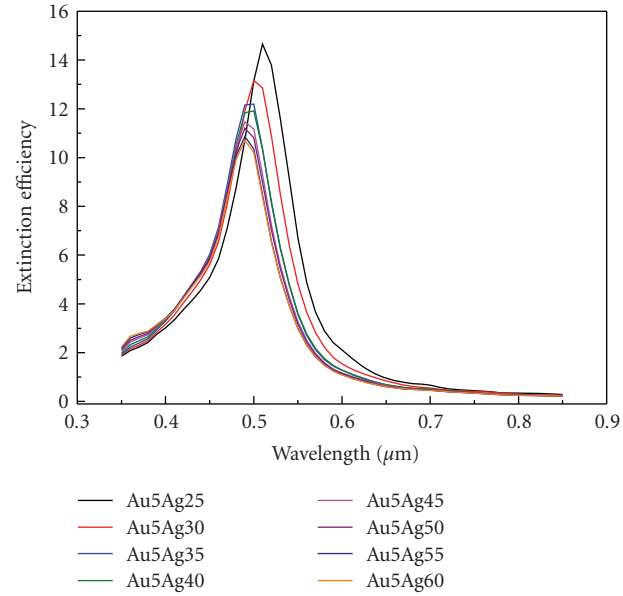

Figure 2: Extinction spectra of fixed Au thickness 5 nm with different Ag thicknesses (varying from 25 to 60 nm) for the rhombic Au-Ag nanostructure array. From [33].

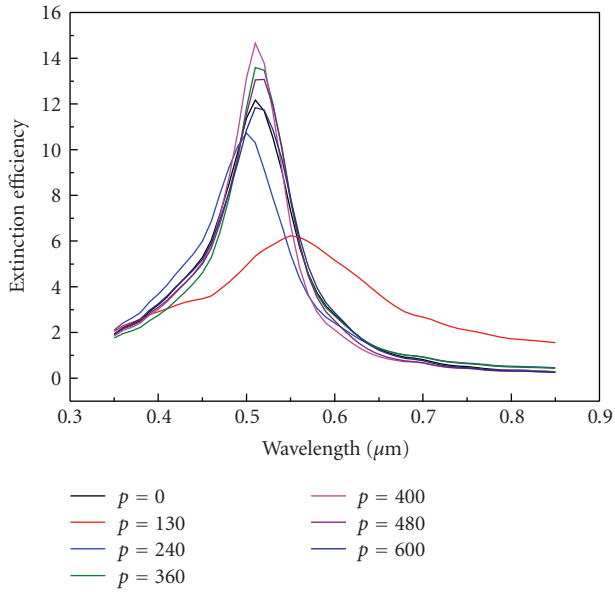

Figure 3: Extinction spectra of different periods (p) for the rhombic Au-Ag nanostructures array. From [33].

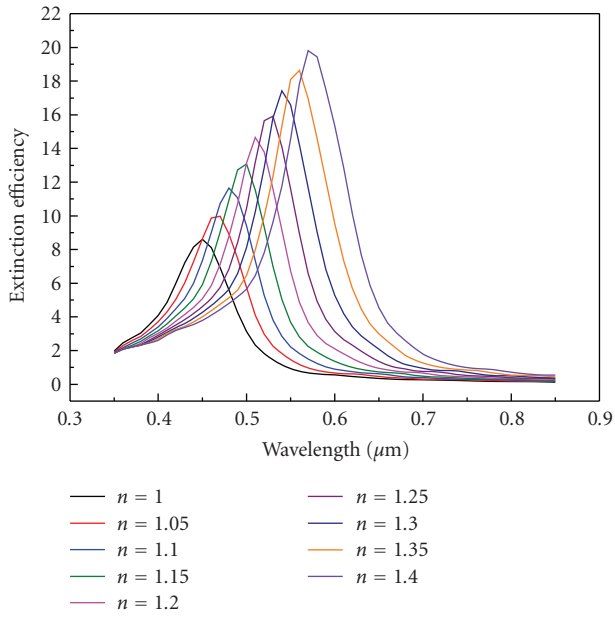

Figure 4: Extinction spectra for different effective refractive indexes mediums surrounding the Au-Ag rhombic nanostructures array. From [33].

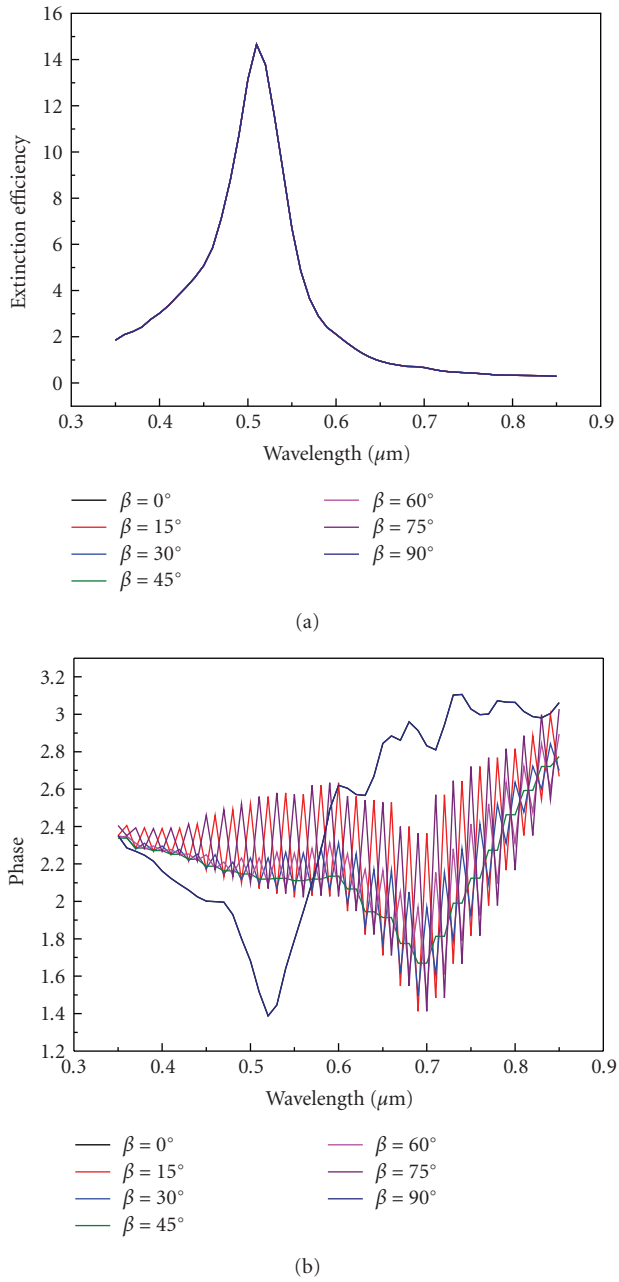

Figure 5: (a) Extinction spectra of different polarizations of the incident light for the rhombic Au-Ag nanostructures. (b) Phase distribution of the different polarizations of the incident light for the rhombic Au-Ag nanostructures. From [33].

The DDA calculations confirm that the material and the structure of nanoparticles have significant effects on their optical extinction spectrum properties. The thickness, the period and the refractive index change of Au and Ag can significantly shift the plasmon peaks. DDA is an effective method to design the structure parameters, which can help us to obtain the suitable structure parameters. The DDA calculated results showed that the nanostructures array formed by identical Au-Ag rhombic nanostructures with in-plane width of about 120 nm and out-of-plane height of about 25 nm Ag and 5 nm Au, and the period of the Au-Ag nanorhombus array 400 nm are suitable structure parameters and the nanostructure array can be used for the potential biological nanosensor application in the future.

2.2. Mathematical Background and Calculated Results of FDTD. FDTD is a computational method based on numerically evaluating the temporal evolution of electromagnetic fields using Maxwell's equations. Because Maxwell's

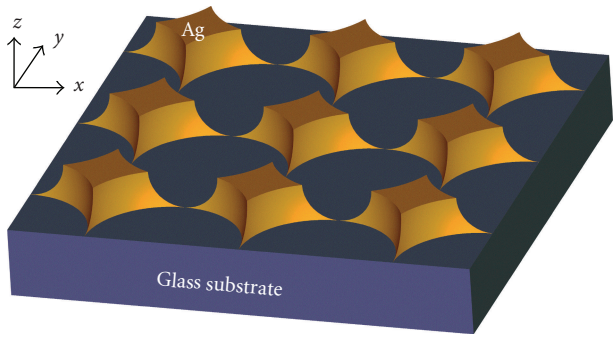

Figure 6: The symmetrical two-dimensional infinite rhombic nanostructures array. From [34].

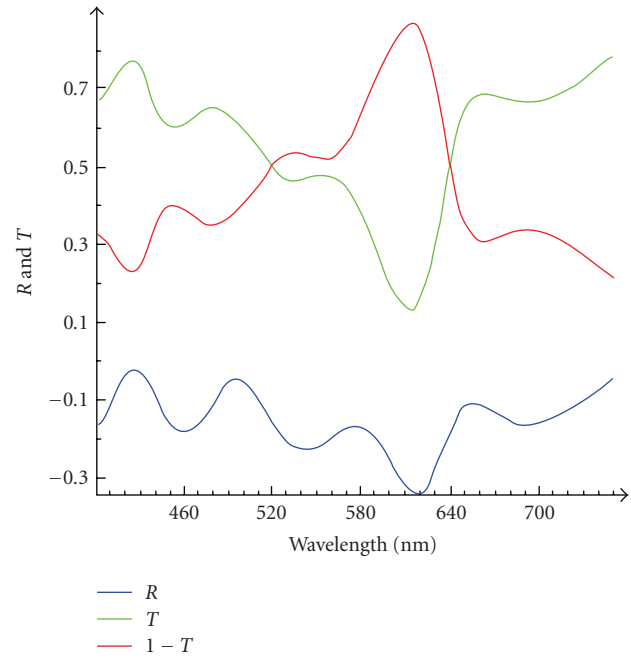

Figure 7: The reflectivity and transmission index of the rhombic nanostructure array calculated by FDTD. From [34].

equations relate time-dependent changes in the electric (magnetic) fields to spatial variations in the magnetic (electric) fields, FDTD programs implement an explicit time-marching algorithm for solving Maxwell's curl equations, usually on an offset Cartesian spatial grid. Modelling a new system is therefore reduced to grid generation, instead of deriving geometry-specific equations. In addition, the time-marching aspect of the FDTD method enables direct observations to be made of both near- and far-field values of the electromagnetic fields at any time during the simulation. With these "snap shots", the time evolution of the electromagnetic fields can be calculated directly. FDTD method treats Maxwell equations as s set of finite-difference equations in both time and space. The model space considered includes both the probe and the sample surface and consists of an aggregation of cubic cells with each cell having its own complex dielectric constant. The finite-difference equations can be written as [23]:

$$\begin{aligned}
&\frac{H_{z(t;x,y+\Delta y,z)} - H_{z(t;x,y-\Delta y,z)}}{2\Delta y} - \frac{H_{y(t;x,y,z+\Delta z)} - H_{y(t;x,y,z-\Delta z)}}{2\Delta z} \\
&\quad = \widetilde{\varepsilon}(x,y,z)\frac{E_{x(t+\Delta t;x,y,z)} - E_{x(t-\Delta t;x,y,z)}}{2\Delta t}, \\
&\frac{H_{x(t;x,y,z+\Delta z)} - H_{x(t;x,y,z-\Delta z)}}{2\Delta z} - \frac{H_{z(t;x+\Delta x,y,z)} - H_{z(t;x-\Delta x,y,z)}}{2\Delta x} \\
&\quad = \widetilde{\varepsilon}(x,y,z)\frac{E_{y(t+\Delta t;x,y,z)} - E_{y(t-\Delta t;x,y,z)}}{2\Delta t}, \\
&\frac{H_{y(t;x+\Delta x,y,z)} - H_{y(t;x-\Delta x,y,z)}}{2\Delta x} - \frac{H_{x(t;x,y+\Delta y,z)} - H_{x(t;x,y-\Delta y,z)}}{2\Delta y} \\
&\quad = \widetilde{\varepsilon}(x,y,z)\frac{E_{z(t+\Delta t;x,y,z)} - E_{z(t-\Delta t;x,y,z)}}{2\Delta t},
\end{aligned} \tag{8}$$

where $E = E(E_x, E_y, E_z)$ and $H = H(H_x, H_y, H_z)$ are the electric field and the magnetic induction vectors, respectively, and $2\Delta x$, $2\Delta y$, and $2\Delta z$ are increments along the three coordinate directions respectively, Δt is the unit time increment, and $\widetilde{\varepsilon}(x, y, z)$ is the complex dielectric constant of the medium at that point. Equation (8) is simultaneously solved to determine the component values at the time $t + \Delta t$. Commercial professional software was adopted here for the computational calculation and numerical analysis [24]. Broad band of the incident light is ranging from 400 nm to 750 nm with plane wave in normal incidence angle $\theta = 0°$. Meshing size in x and y (two-dimensional simulation) is $\Delta x = 2$ nm and $\Delta y = 2$ nm, respectively. Simulation time t (theoretically, $t = \Delta x/2c$, c is the velocity of light) is set to be 125 fs. The output result is the relationship between the absorption and the incident wavelength.

The FDTD has become an extremely powerful technique for modelling nanostructures with complex shapes as well as arrangements of multiple nanostructures. By using FDTD, we proposed a design approach of metallic nanoparticles for biosensing: calculation of electronic-field enhancement. The engineered rhombic Ag nanostructures array was designed by means of finite-difference and time-domain (FDTD) algorithm-based computational numerical calculation through both spectrum and electromagnetic field analyses [34]. The extinction efficiency was obtained by theoretical numerical calculation. Moreover, the LSPR-induced enhancement of the electronic field distribution is calculated. All the rhombic nanostructure array and the calculated results are shown in Figures 6, 7, 8, and 9. It can be seen from the figures that the rhombic Ag nanostructures array can enhance the localized electric fields near the surface of the metallic array. This design approach may be a guideline for designing the engineered metallic particles arrays.

3. Nanofabrication Techniques

Nanostructured metallic arrays have attracted considerable attention of researchers because of their broad applications in nanoscience and nanotechnology such as enhanced Raman

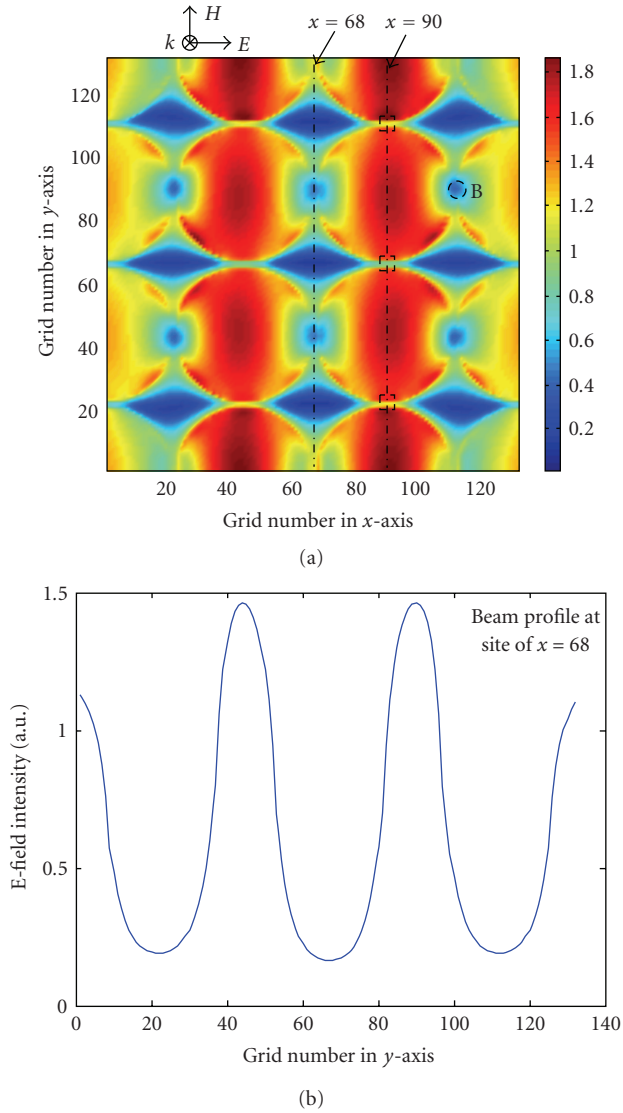

Figure 8: (a) Electronic field distribution (x-y plane) above 5 nm from the surface of the Ag rhombic nanostructure calculated by FDTD. (b) Electronic field curve at the center of the array at site of $x = 68$. From [34].

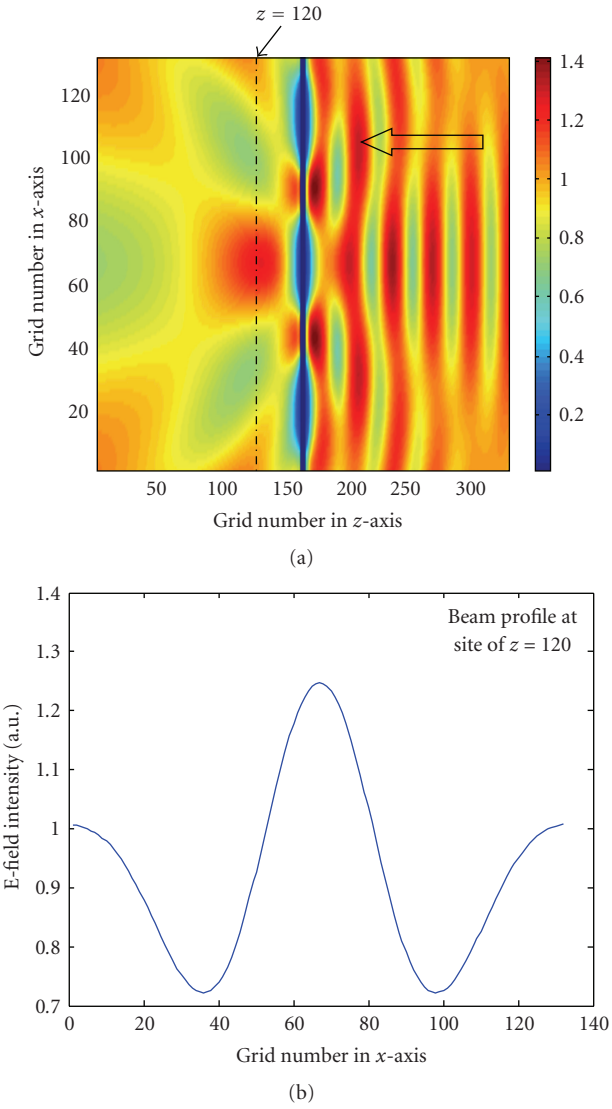

Figure 9: (a) Electronic field distribution (x-z plane, y located at the center of the array) of the Ag rhombic nanostructure calculated by FDTD. The arrow indicates propagation direction. (b) Electronic field curve at the center of the array at site of $z = 120$ nm. From [34].

scattering [35], bioreactors [36], and biosensors [37–40], Nanostructured arrays may be produced using many different methods, including electron beam lithography [41], ion beam lithography [42], focused ion beam (FIB) [26, 43], X-ray lithography [44], electron holographic lithography [45], laser interference lithography [46] and nanosphere lithography (NSL) [25]. Among these techniques, NSL and FIB are increasingly used in research laboratories [47]. NSL techniques developed by Van Duyne's group [48, 49] began with the deposition of polystyrene(PS) nanospheres by drop-casting them onto a solid substrate and allowing them to self-assemble into hexagonally close-packed monolayers. The PS nanospheres act as masks in subsequent physical vapor deposition of noble metal. Then the PS nanosphere mask was removed by sonicating in solvent to obtain the triangular nanostructure array. While FIB allows direct patterning and therefore does not require an intermediate sensitive media or process (resist, metal deposited film, etching process). Around 1959, Feynman asked the question on the FIB fabrication limits of miniaturization [50]. He proposed to use ion beams to sculpt matter to the required nanoscale. The realization of features fabricated using FIB lithography with lateral widths as small as 8 nm in a poly (methyl methacrylate) (PMMA) resist layer was in particular demonstrated by the team of Seliger and then later of Kubena [51]. Recently, Arshak [52, 53] proposed a new lithographical concept about FIB lithography capabilities. This concept organizes a bilayer resist on a substrate. The first layer is irradiated with gallium ions to paint a mask pattern. Then the image of the gallium implanted mask is transferred to the

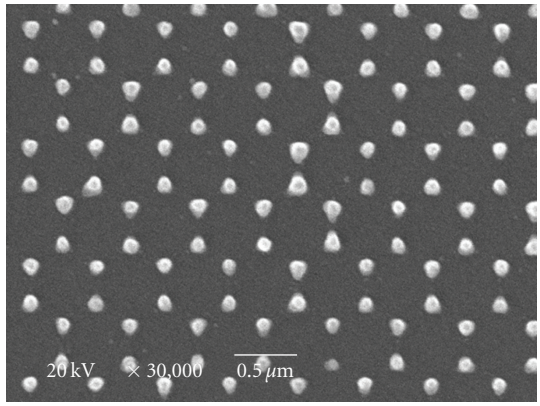

Figure 10: SEM image of topography of the triangular nanostructures array fabricated using NSL. From [55].

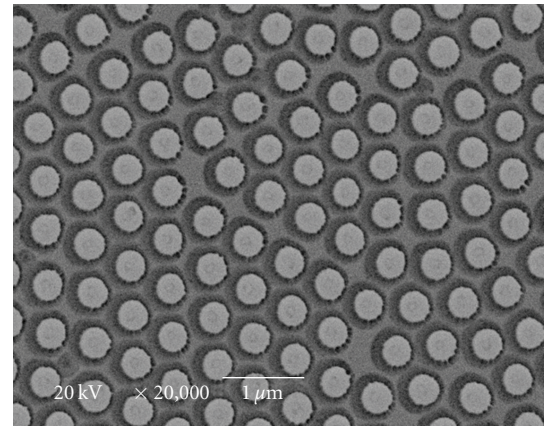

Figure 12: SEM image of hexagonal-arranged Au nanocolumn array fabricated using RIE-NSL. From [55].

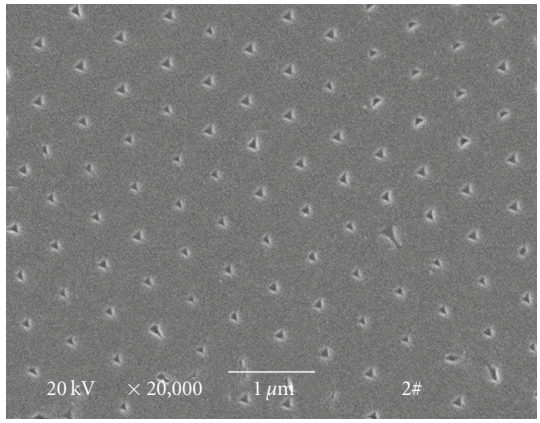

Figure 11: SEM image of triangular-arranged hexagonal array fabricated using NSL. From [55].

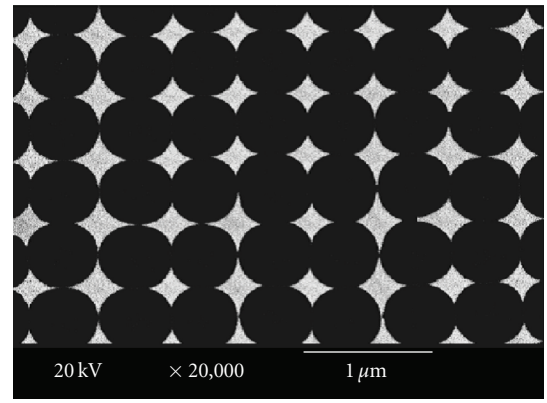

Figure 13: SEM image of rhombic silver nanostructure array fabricated using RIE-NSL. From [55].

second resist layer using a dry reactive ion etching process of oxygen (O_2). This technique can fabricate deep sub-100 nm features and high aspect ratio resist features (up to 21 : 1). It is suitable for many application fields requiring high resolution and high aspect ratio lithography.

However, using NSL alone can generate only a few limited patterns [54]. The close-packed submicron spheres used as masks in the NSL form hexagonal-arranged triangular interstice arrays only in the monolayer. Because NSL has potential for producing a well-ordered, two-dimensional (2D) periodic nanoparticle arrays from a wide variety of materials on different substrates, some of the relevant works have received much attention at present.

To overcome the problem of generating a few limited patterns, we describe an alternative approach that combines reactive ion etching (RIE) with NSL techniques to achieve more varieties of nanostructure arrays [55]. We refer to this reactive ion etching-assisted nanosphere lithography technique as RIE-NSL. Specifically, RIE is used to tune the shape and size of a monolayer or bilayer of submicron spheres after the NSL process. As a result, the nanostructured metallic arrays with different shapes and sizes are formed on the substrates by subsequent RIE etching and deposition processes using the spheres as masks. To illustrate this method, we fabricated several different shapes such as nanorhombic, nanohexagon, and nanocolumn arrays on glass substrate. During this fabrication process, the hemispheroidal polystyrene (PS) arrays and porous Ag membranes have also been obtained. Using NSL technology, we have fabricated the triangular, rhombic, hexagonal, column, and so forth, nanostructure arrays, as shown in the SEM images in Figures 10, 11, 12, and 13.

FIB is a technique used particularly in the semiconductor and materials science fields for site-specific analysis, deposition, and ablation of materials. An FIB setup is a scientific instrument that resembles a scanning electron microscope (SEM). However, while the SEM uses a focused beam of electrons to image the sample in the chamber, an FIB setup instead uses a focused beam of ions.

We have carried out considerable work in the area of FIB nanofabrication and geometrical characterization [56–58] and succeeded in producing various nanostructures including nanodots, nanorods, nanowells, and nanoscale gratings, as shown in Figure 14. Our researches cover not

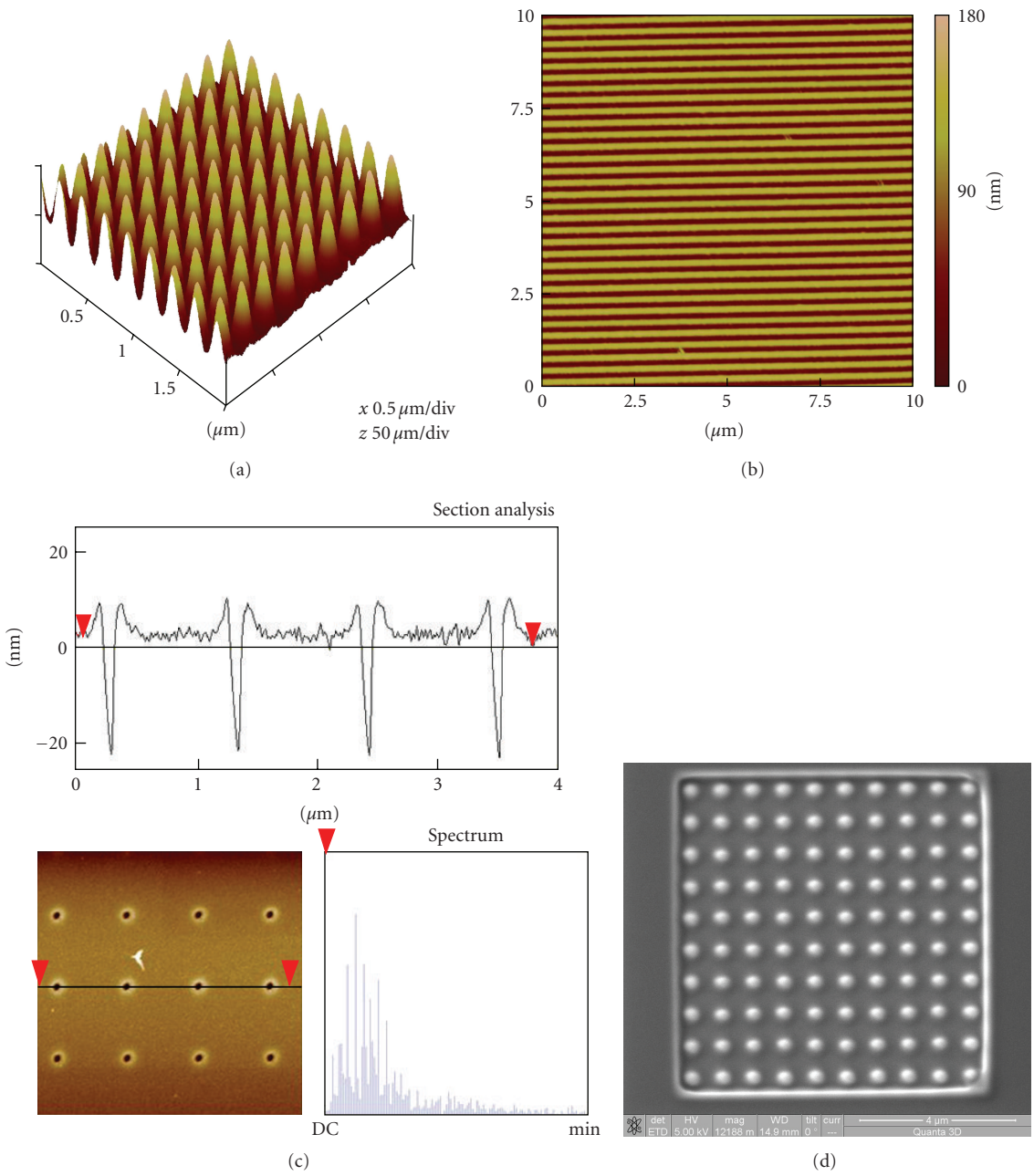

Figure 14: Various nanostructures produced with FIB. (a) Nanopillars; (b) Nanoscale gratings; (c) Nanowells; and (d) Nanodots. From [57, 58].

only FIB direct nanofabrication but also FIB-induced self-organization of nanostructures and template-guided self-organization. The understanding of self-organization makes it possible to produce self-organized nanostructures if they are useful or suppress the undesirable self-organization in the process of direct nanofabrication.

4. Refractive-Index Plasmonic Sensing

The LSPR-based nanobiosensor is a refractive index-based sensing device which relies on the extraordinary optical properties of noble metal (e.g., Ag, Au and Cu) nanoparticles [59, 60]. The sensing capability of the LSPR sensor can be modified by tuning shape, size and material composition of the nanoparticles. The nanoparticles are effective for quantitative detection of chemical and biological targets [61]. The sensing principle employed in these experiments relies on the high sensitivity of the LSPR spectrum of the noble metal nanoparticles due to an absorbate-induced change in the dielectric constant of the surrounding environment. The local environment that surrounds the nanoparticles can be modified by chemic disposal and the binding of the biological molecular. The extinction spectrum of the

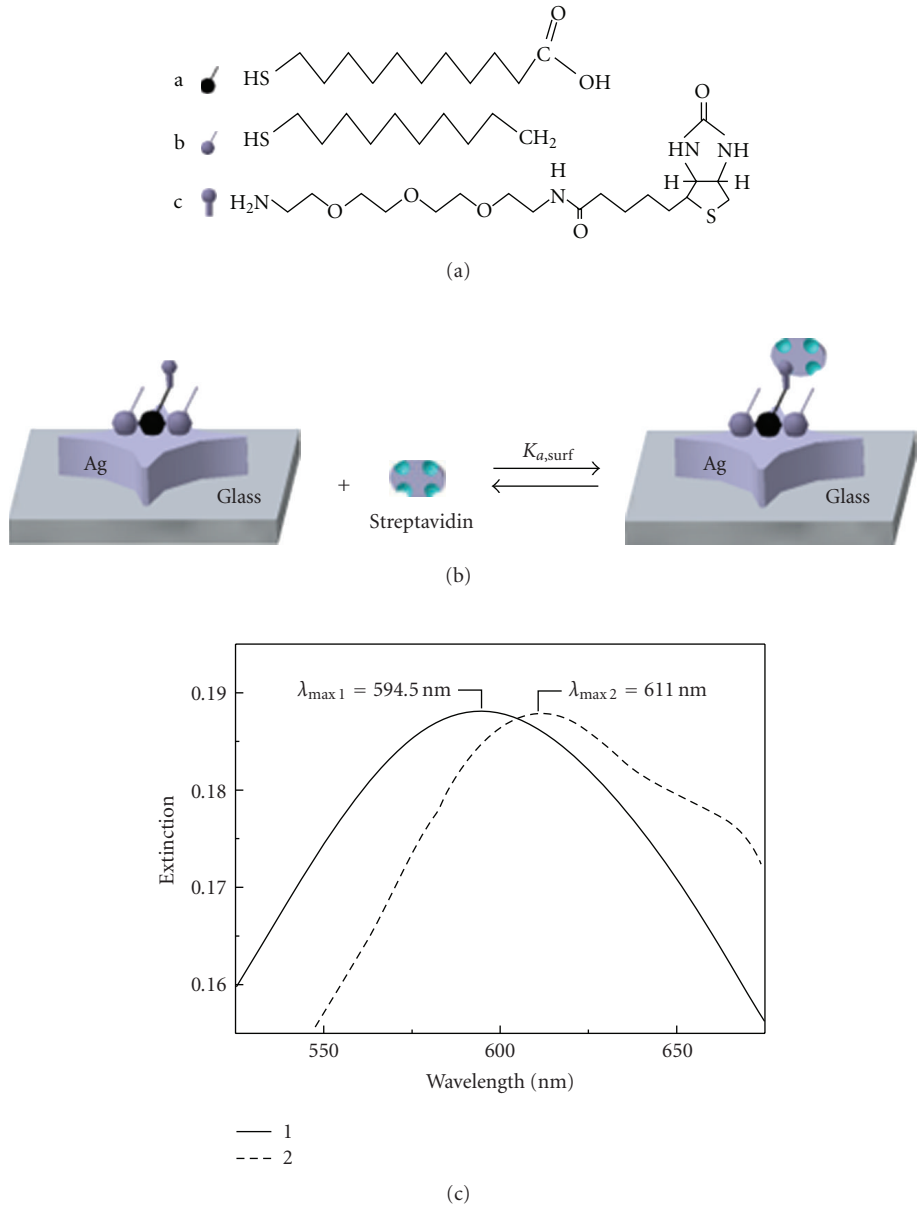

Figure 15: A nanoscale biosensor based on LSPR sensitivity to local medium dielectric change. (a) Scheme showing the formation of thiol monolayer on the nanotriangles followed by their conjugation to biotin molecules via free carboxylic acid groups, three chemical structures of case a, 11-Mercaptoundecanoic (11-MUA); case b, 1-octanethiol (1-OT); case c, biotin. (b) Scheme showing the binding of streptavidin molecules to the biotinylated nanorhombics on the substrate. (c) LSPR extinction spectrum of the Ag nanobiosensor (1) before and (2) after exposure to 100 nM streptavidin. From [62].

nanosensor can be derived using a spectrophotometer [4]. Figure 15 shows a nanoscale biosensor based on surface plasmon resonance sensitivity to local medium dielectric changes [62]. LSPR spectra of each step in the surface modification of NSL-derived Ag nanoparticles to form a biotinylated Ag nano-biosensor and the specific binding of SA is shown in Figure 16 [62]. We used our designed nanobiosensor to probe antibody antigen interactions and even diagnose Alzheimer's disease (ADDLs-potential Alzheimer's disease (AD) biomarkers) [63] and the SEB infection [64].

5. Summary

In this review, we discuss the enhanced optical properties of noble metal nanoparticles, with an emphasis on the recent advances in the utility of these plasmonic properties in the theory background, fabrication method, plasmonic sensing and plasmonic waveguides. The DDA and FDTD method applied brute-force computational methods for different nanoparticles optical properties. The nanostructure fabrication technologies such as FIB, NSL are two important

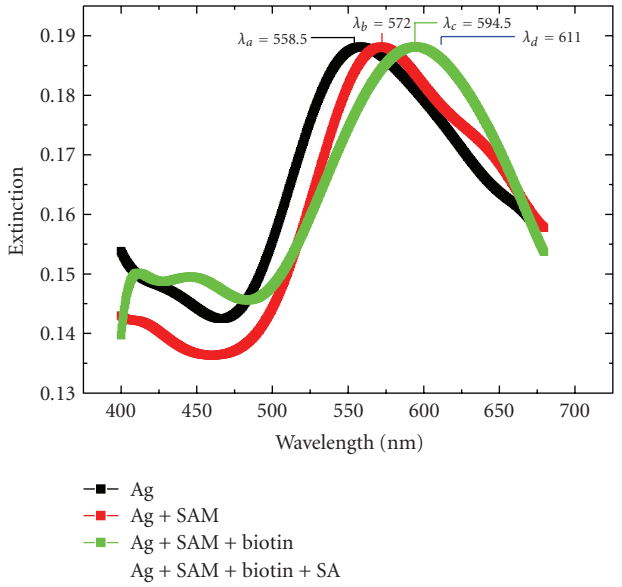

(a)

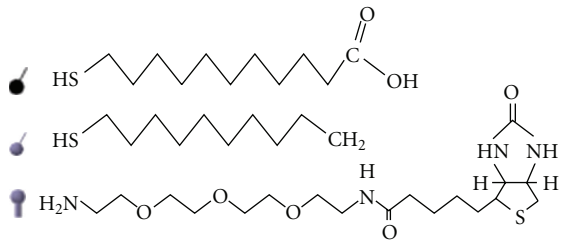

(b)

Figure 16: LSPR spectra of each step in the surface modification of NSL-derived Ag nanoparticles to form a biotinylated Ag nanobiosensor and the specific binding of SA. (a) Ag nanoparticles before chemical modification, k_{max} = 558.5 nm. (b) Ag nanoparticles modified by 1 mM 1:3 11-MUA/1-OT, λ_{max} = 572 nm. (c) Ag nanoparticles after modification with 1mM biotin, λ_{max} = 594.5 nm. (d) Ag nanoparticles associated with 100 nM SA, λ_{max} = 611 nm. All extinction measurements were collected in air environment. From [62].

methods to fabricate the nanostructures. They can fabricate arbitrary shapes nanostructures. Moreover, in the application of the LSPR nanobiosensor, we focus on the application of detecting the binding signal between the antibody and antigen, ADDL, and SEB in nM concentration level. In the future, we will proceed to the single molecule detection method based on the LSPR.

Acknowledgments

The authors acknowledge financial support by A*STAR (Agency for Science, Technology, and Research), Singapore, under SERC Grant no. 072 101 0023.

References

[1] C. L. Haynes, A. D. McFarland, L. Zhao, et al., "Nanoparticle optics: the importance of radiative dipole coupling in two-dimensional nanoparticle arrays," *Journal of Physical Chemistry B*, vol. 107, no. 30, pp. 7337–7342, 2003.

[2] C. L. Haynes and R. P. Van Duyne, "Dichroic optical properties of extended nanostructures fabricated using angle-resolved nanosphere lithography," *Nano Letters*, vol. 3, no. 7, pp. 939–943, 2003.

[3] P. C. Andersen and K. L. Rowlen, "Brilliant optical properties of nanometric noble metal spheres, rods, and aperture arrays," *Applied Spectroscopy*, vol. 56, pp. 124A–135A, 2002.

[4] A. J. Haes, S. Zou, G. C. Schatz, and R. P. Van Duyne, "A nanoscale optical biosensor: the long range distance dependence of the localized surface plasmon resonance of noble metal nanoparticles," *Journal of Physical Chemistry B*, vol. 108, no. 1, pp. 109–116, 2004.

[5] T. Jensen, L. Kelly, A. Lazarides, and G. C. Schatz, "Electrodynamics of noble metal nanoparticles and nanoparticle clusters," *Journal of Cluster Science*, vol. 10, no. 2, pp. 295–317, 1999.

[6] T. R. Jensen, M. D. Malinsky, C. L. Haynes, and R. P. Van Duyne, "Nanosphere lithography: tunable localized surface plasmon resonance spectra of silver nanoparticles," *Journal of Physical Chemistry B*, vol. 104, no. 45, pp. 10549–10556, 2000.

[7] A. M. Michaels, M. Nirmal, and L. E. Brus, "Surface enhanced Raman spectroscopy of individual rhodamine 6G molecules on large Ag nanocrystals," *Journal of the American Chemical Society*, vol. 121, no. 43, pp. 9932–9939, 1999.

[8] S. Schultz, D. R. Smith, J. J. Mock, and D. A. Schultz, "Single-target molecule detection with nonbleaching multicolor optical immunolabels," *Proceedings of the National Academy of Sciences of the United States of America*, vol. 97, no. 3, pp. 996–1001, 2000.

[9] J. Yguerabide and E. E. Yguerabide, "Light-scattering submicroscopic particles as highly fluorescent analogs and their use as tracer labels in clinical and biological applications I. Theory," *Analytical Biochemistry*, vol. 262, no. 2, pp. 137–156, 1998.

[10] J. Yguerabide and E. E. Yguerabide, "Light-scattering submicroscopic particles as highly fluorescent analogs and their use as tracer labels in clinical and biological applications II. Experimental characterization," *Analytical Biochemistry*, vol. 262, no. 2, pp. 157–176, 1998.

[11] G. C. Schatz and R. P. Van Duyne, "Electromagnetic mechanism of surface-enhanced spectroscopy," in *Handbook of Vibrational Spectroscopy*, J. M. Chalmers and P. R. Griffiths, Eds., vol. 1, pp. 759–774, John Wiley & Sons, New York, NY, USA, 2002.

[12] T. A. Taton, C. A. Mirkin, and R. L. Letsinger, "Scanometric DNA array detection with nanoparticle probes," *Science*, vol. 289, no. 5485, pp. 1757–1760, 2000.

[13] C. A. Mirkin, R. L. Letsinger, R. C. Mucic, and J. J. Storhoff, "A DNA-based method for rationally assembling nanoparticles into macroscopic materials," *Nature*, vol. 382, no. 6592, pp. 607–609, 1996.

[14] U. Kreibig and M. Vollmer, *Optical Properties of Metal Clusters*, vol. 25, Springer, Heidelberg, Germany, 1995.

[15] T. Linnert, P. Mulvaney, and A. Henglein, "Surface chemistry of colloidal silver: surface plasmon damping by chemisorbed I-, SH-, and C6H5S-," *Journal of Physical Chemistry*, vol. 97, no. 3, pp. 679–682, 1993.

[16] H. Takei, "Biological sensor based on localized surface plasmon associated with surface-bound Au/polystyrene composite microparticles," in *Microfluidic Devices and Systems*, vol. 3515 of *Proceedings of SPIE*, pp. 278–283, Santa Clara, Calif, USA, September 1998.

[17] A. J. Haes and R. P. Van Duyne, "A nanoscale optical biosensor: sensitivity and selectivity of an approach based on the localized surface plasmon resonance spectroscopy of triangular silver nanoparticles," *Journal of the American Chemical Society*, vol. 124, no. 35, pp. 10596–10604, 2002.

[18] A. J. Haes and R. P. Van Duyne, "Nanosensors enable portable detectors for environmental and medical applications," *Laser Focus World*, vol. 39, no. 5, pp. 153–156, 2003.

[19] T. A. Taton, G. Lu, and C. A. Mirkin, "Two-color labeling of oligonucleotide arrays via size-selective scattering of nanoparticle probes," *Journal of the American Chemical Society*, vol. 123, no. 21, pp. 5164–5165, 2001.

[20] Y. Cao, R. Jin, and C. A. Mirkin, "DNA-modified core-shell Ag/Au nanoparticles," *Journal of the American Chemical Society*, vol. 123, no. 32, pp. 7961–7962, 2001.

[21] R. Jin, Y. W. Cao, C. A. Mirkin, K. L. Kelly, G. C. Schatz, and J. G. Zheng, "Photoinduced conversion of silver nanospheres to nanoprisms," *Science*, vol. 294, no. 5548, pp. 1901–1903, 2001.

[22] G. C. Schatz, "Electrodynamics of nonspherical noble metal nanoparticles and nanoparticle aggregates," *Journal of Molecular Structure: THEOCHEM*, vol. 573, no. 1–3, pp. 73–80, 2001.

[23] S. Kawata, M. Ohtsu, and M. Irie, Eds., *Nano-Optics*, chapter 2, Springer, Heidelberg, Germany, 2002.

[24] A commercial software developed by a company: Lumerical Inc., http://www.lumerical.com/.

[25] X. Zhang and R. P. Van Duyne, "Optimized silver film over nanosphere surfaces for the biowarfare agent detection based on surface-enhanced Raman spectroscopy," in *Materials Research Society Symposium Proceedings*, vol. 876, pp. 207–212, San Francisco, Calif, USA, March 2005.

[26] H. X. Qian, W. Zhou, J. Miao, L. E. N. Lim, and X. R. Zeng, "Fabrication of Si microstructures using focused-ion-beam implantation and reactive ion etching," *Journal of Micromechanics and Microengineering*, vol. 18, no. 3, Article ID 035003, 5 pages, 2008.

[27] Y. Q. Fu, W. Zhou, L. E. N. Lim, et al., "Influence of V-shaped plasmonic nanostructures on beam propagation," *Applied Physics B*, vol. 86, no. 3, pp. 461–466, 2007.

[28] G. Mie, "Beiträge zur optik trüber medien, speziell kolloidaler metallösungen," *Annals of Physics*, vol. 25, pp. 377–445, 1908.

[29] A. L. Aden and M. Kerker, "Scattering of electromagnetic waves from two concentric spheres," *Journal of Applied Physics*, vol. 22, no. 10, pp. 1242–1246, 1951.

[30] B. T. Draine and P. J. Flatau, "Discrete-dipole approximation for scattering calculations," *Journal of the Optical Society of America A*, vol. 11, no. 4, pp. 1491–1499, 1994.

[31] M. Futamata, Y. Maruyama, and M. Ishikawa, "Local electric field and scattering cross section of Ag nanoparticles under surface plasmon resonance by finite difference time domain method," *Journal of Physical Chemistry B*, vol. 107, no. 31, pp. 7607–7617, 2003.

[32] B. T. Draine and P. J. Flatau, "User guide for the discrete dipole approximation code DDSCAT 6.1," preprint, 2004, http://arxiv.org/abs/astro-ph/0409262.

[33] S. L. Zhu and W. Zhou, "Optical characteristics of rhombic hybrid Au-Ag nanostructures calculated by discrete dipole approximation method," *Journal of Computational and Theoretical Nanoscience*, vol. 7, no. 3, pp. 634–637, 2010.

[34] S. L. Zhu and Y. Q. Fu, "Design approach of metallic nanoparticles for biosensing: calculation of electronic-field enhancement," *Journal of Computational and Theoretical Nanoscience*, vol. 17, no. 1-6, 2010.

[35] H. W. Deckman and J. H. Dunsmuir, "Applications of surface textures produced with natural lithography," *Journal of Vacuum Science and Technology B*, vol. 1, no. 4, pp. 1109–1112, 1983.

[36] K. Sato, Y. Kawamura, S. Tanaka, K. Uchida, and H. Kohida, "Individual and mass operation of biological cells using micromechanical silicon devices," *Sensors and Actuators A*, vol. 23, no. 1–3, pp. 948–953, 1990.

[37] C. R. Musil, D. Jeggle, H. W Lehmann, L. Scandella, J. Gobrecht, and M. Dobeli, "Nanostructuring of gold electrodes for immunosensing applications," *Journal of Vacuum Science and Technology B*, vol. 13, pp. 2781–2786, 1995.

[38] S. Zhu, F. Li, C. Du, and Y. Q. Fu, "A localized surface plasmon resonance nanosensor based on rhombic Ag nanoparticle array," *Sensors and Actuators B*, vol. 134, no. 1, pp. 193–198, 2008.

[39] S. Zhu, F. Li, C. Du, and Y. Q. Fu, "Novel bio-nanochip based on localized surface plasmon resonance spectroscopy of rhombic nanoparticles," *Nanomedicine*, vol. 3, no. 5, pp. 669–677, 2008.

[40] S. Zhu, C. Du, and Y. Q. Fu, "Biochemistry nanosensor-based hybrid metallic nanostructures array," *Sensors and Actuators B*, vol. 137, no. 1, pp. 345–349, 2009.

[41] S. Y. Chou, M. S. Wei, P. R. Krauss, and P. B. Fischer, "Single-domain magnetic pillar array of 35 nm diameter and 65 Gbits/in.^{2} density for ultrahigh density quantum magnetic storage," *Journal of Applied Physics*, vol. 76, no. 10, pp. 6673–6675, 1994.

[42] J. C. Wolfe, S. V. Pendharkar, P. Ruchhoeft, et al., "A proximity ion beam lithography process for high density nanostructures," *Journal of Vacuum Science and Technology B*, vol. 14, no. 6, pp. 3896–3899, 1996.

[43] Y. Q. Fu, W. Zhou, L. E. N. Lim, et al., "Influence of V-shaped plasmonic nanostructures on beam propagation," *Applied Physics B*, vol. 86, no. 3, pp. 461–466, 2007.

[44] Y. Chen, R. K. Kupka, F. Rousseaux, et al., "50-nm X-ray lithography using synchrotron radiation," *Journal of Vacuum Science & Technology B*, vol. 12, no. 6, pp. 3959–3964, 1994.

[45] K. Ogai, Y. Kimura, R. Shimizu, J Fujita, and S. Matsui, "Nanofabrication of grating and dot patterns by electron holographic lithography," *Applied Physics Letters*, vol. 66, no. 12, pp. 1560–1562, 1995.

[46] J. P. Spallas, R. D. Boyd, J. A. Britten, et al., "Fabrication of sub-0.5 μm diameter cobalt dots on silicon substrates and photoresist pedestals on 50 cm $\times$ 50 cm glass substrates using laser interference lithography," *Journal of Vacuum Science and Technology B*, vol. 14, no. 3, pp. 2005–2007, 1996.

[47] X. D. Wang, E. Graugnard, J. S. King, Z. L. Wang, and C. J. Summers, "Large-scale fabrication of ordered nanobowl arrays," *Nano Letters*, vol. 4, no. 11, pp. 2223–2226, 2004.

[48] J. C. Hulteen, D. A. Treichel, M. T. Smith, M. L. Duval, T. R. Jensen, and R. P. Van Duyne, "Nanosphere lithography: size-tunable silver nanoparticle and surface cluster arrays," *Journal of Physical Chemistry B*, vol. 103, no. 19, pp. 3854–3863, 1999.

[49] T. R. Jensen, G. C. Schatz, and R. P. Van Duyne, "Nanosphere lithography: surface plasmon resonance spectrum of a periodic array of silver nanoparticles by ultraviolet—visible extinction spectroscopy and electrodynamic modeling," *Journal of Physical Chemistry B*, vol. 103, no. 13, pp. 2394–2401, 1999.

[50] R. P. Feynman, "There's plenty of room at the bottom—an invitation to enter a new field of physics," 1959, Caltech's Engineering and Science, http://www.zyvex.com/nanotech/feynman.html.

[51] R. L. Kubena, J. W. Ward, F. P. Stratton, R. J. Joyce, and G. M. Atkinson, "Transition metal carbides for use as field emission cathodes," *Journal of Vacuum Science and Technology B*, vol. 9, pp. 3079–3083, 1991.

[52] K. Arshak, M. Mihov, S. Nakahara, A. Arshak, and D. McDonagh, "A novel focused-ion-beam lithography process for sub-100 nanometer technology nodes," *Superlattices and Microstructures*, vol. 36, no. 1–3, pp. 335–343, 2004.

[53] S. F. Gilmartin, K. Arshak, D. Collins, O. Korostynska, and A. Arshak, "Fabricating nanoscale device features using the 2-step NERIME nanolithography process," *Microelectronic Engineering*, vol. 84, no. 5-8, pp. 833–836, 2007.

[54] M. Geissler and Y. Xia, "Patterning: principles and some new developments," *Advanced Materials*, vol. 16, no. 15, pp. 1249–1269, 2004.

[55] S. L. Zhu, Y. Q. Fu, and C. L. Du, "Fabrication and characterization of nanostructured metallic arrays with multi-shapes in monolayer and bilayer," *Journal of Nanoparticle Research*, vol. 12, no. 5, pp. 1829–1835, 2010.

[56] J. Lian, W. Zhou, Q. M. Wei, L. M. Wang, L. A. Boatner, and R. C. Ewing, "Simultaneous formation of surface ripples and metallic nanodots induced by phase decomposition and focused ion beam patterning," *Applied Physics Letters*, vol. 88, no. 9, Article ID 093112, 3 pages, 2006.

[57] Y. Q. Fu, N. K. A. Bryan, and W. Zhou, "Quasi-direct writing of diffractive structures with a focused-ion-beam," *Optics Express*, vol. 12, no. 9, pp. 1803–1809, 2004.

[58] Y. Q. Fu, W. Zhou, L. E. N. Lim, et al., "Geometrical characterization issues of plasmonic nanostructure with depth-tuned grooves for beam shaping," *Optical Engineering*, vol. 45, no. 10, Article ID 108001, 2006.

[59] C. R. Yonzon, E. Jeoung, S. Zou, G. C. Schatz, M. Mrksich, and R. P. Van Duyne, "A comparative analysis of localized and propagating surface plasmon resonance sensors: the binding of concanavalin a to a monosaccharide functionalized self-assembled monolayer," *Journal of the American Chemical Society*, vol. 126, pp. 12669–12676, 2004.

[60] J. C. Riboh, A. J. Haes, A. D. McFarland, C. R. Yonzon, and R. P. Van Duyne, "A nanoscale optical biosensor: real-time immunoassay in physiological buffer enabled by improved nanoparticle adhesion," *Journal of Physical Chemistry B*, vol. 107, no. 8, pp. 1772–1780, 2003.

[61] J. Yuan, R. Oliver, J. Li, J. Lee, M. Aguilar, and Y. Wu, "Sensitivity enhancement of SPR assay of progesterone based on mixed self-assembled monolayers using nanogold particles," *Biosensors and Bioelectronics*, vol. 23, no. 1, pp. 144–148, 2007.

[62] S. Zhu, C. Du, and Y. Q. Fu, "Fabrication and characterization of rhombic silver nanoparticles for biosensing," *Optical Materials*, vol. 31, no. 6, pp. 769–774, 2009.

[63] S. Zhu, C. Du, Y. Q. Fu, Q. Deng, and L. Shi, "Influence of Cr adhesion layer on detection of amyloid-derived diffusible ligands based on localized surface plasmon resonance," *Plasmonics*, vol. 4, no. 2, pp. 135–140, 2009.

[64] S. Zhu, C. Du, and Y. Q. Fu, "Localized surface plasmon resonance-based hybrid Au-Ag nanoparticles for detection of Staphylococcus aureus enterotoxin B," *Optical Materials*, vol. 31, no. 11, pp. 1608–1613, 2009.